

Mixed convection heat transfer in a lid-driven trapezoidal enclosure filled with nanofluids

Ali Khaleel Kareem ^{a, b,*}, H. A. Mohammed ^c, Ahmed Kadhim Hussein ^d, Shian Gao ^a

^a Department of Engineering, University of Leicester, Leicester LE1 7RH, United Kingdom

^b Engineering Department, University of Thi-Qar, Nassiriya, Iraq

^c Department of Thermofluids, Faculty of Mechanical Engineering, Universiti Teknologi Malaysia, 81310 UTM Skudai, Johor Bahru, Malaysia

^d Department of Mechanical Engineering, College of Engineering, Babylon University, Babylon City, Iraq

Abstract

Mixed convection heat transfer in a two-dimensional trapezoidal lid-driven enclosure filled with nanofluids heated from below is numerically studied. The governing equations for both fluid flow and heat transfer are solved by using the finite volume method (FVM). The bottom wall of the enclosure is heated while the upper wall is cooled at lower temperature and the other two sidewalls are adiabatic. Four types of nanofluids (Al_2O_3 , CuO , SiO_2 , and TiO_2 with pure water) with nanoparticles volume fraction (ϕ) in the range of 1 - 4% and nanoparticles diameter in the range 25 - 70 nm were used. This investigation covers Richardson number and Reynolds number in the ranges of 0.1 - 10 and 100-1200, respectively. The trapezoidal lid-driven enclosure was studied for different rotational angles (Φ) in the range of 30° - 60° , different inclination sidewalls angles (γ) in the range of 30° - 60° and various aspect ratios (A) ranged from 0.5 - 2. This investigation is also examined the opposing and aiding flow conditions. The results show that all types of nanofluids have higher Nusselt number compared with pure water. It is found that SiO_2 -water has the highest Nusselt number followed by Al_2O_3 -water, TiO_2 -water, and CuO -water. The Nusselt number increases as the volume fraction increases but it decreases as the diameter of the nanoparticles of nanofluids increases. The Nusselt number increases with the decrease of rotational angle and inclination angle from 30° - 60° and with the increase of aspect ratio. The results of flow direction show that the aiding flow gives higher Nusselt number than the opposing flow.

Keywords: Mixed convection, Heat transfer, Lid driven, Trapezoidal Enclosure, Nanofluids.

*Corresponding author at: Department of Engineering, University of Leicester, Leicester LE1 7RH, United Kingdom. Tel.: +44 (0)116 252 2874; fax: +44 (0)116 2522525.
Email address: akkak2@le.ac.uk, alikhaleel17@yahoo.com (A.K. Kareem), Husseindash@yahoo.com (H. A. Mohammed)

Nomenclature

A	Aspect Ratio, H/W
C_p	Specific heat at constant pressure (J/kg K)
d_p	Diameter of nanofluid particles (nm)
G	Gravitational acceleration (m/s^2)
Gr	Grashof number ($g \beta \Delta T W^3 / \nu^2$)
H	Convective heat transfer coefficient ($W/m^2 K$)
K	Thermal conductivity of the fluid (W/m K)
Nu	Nusselt number (hW/k)
Pr	Prandtl number (ν/α)
q''	Heat Flux (W/m^2)
R	Length of the inclined sidewalls (m)
Ra	Rayleigh number ($g \beta \Delta T H^3 / \alpha \nu$)
Re	Reynolds number (uW/ν)
Ri	Richardson number (Gr/Re^2)
T	Temperature of the fluid (K)
U	Velocity component at x-direction (m/s)
U	Dimensionless velocity component at x-direction (u/U_o)
V	Velocity component at y-direction (m/s)
V	Dimensionless velocity component at y-direction (v/U_o)
W	Length of the cavity (m)
X	Distance along the x-coordinate, m
X	Distance along the non-dimensional x-coordinate (x/W)
Y	Distance along the non-dimensional y-coordinate (y/W)

Greek Symbols

A	thermal diffusivity of the fluid (m^2/s)
B	volumetric coefficient of thermal expansion (1/K)
Γ	inclination angle of the sidewalls of the cavity
Θ	dimensionless temperature $(T_H - T_C)/\Delta T$
M	dynamic viscosity of the fluid (Pa s)
N	kinematic viscosity of the fluid (m^2/s)
P	density of the fluid (kg/m^3)
Φ	rotational angle of the cavity
ϕ	volume fraction
E	Nondimensional length of the heat source (1/L)
φ	volume fraction (%)

Subscripts

av	average value
bf	base fluid
C	Cold temperature
dp	nanoparticles diameter
f	Fluid
H	Hot temperature
nf	Nanofluid
p	Nanoparticles
W	Wall

1. Introduction

Mixed convection heat transfer in a lid-driven enclosure had been a subject of interest in many research studies. Mixed convection flow in lid-driven cavities or enclosures occurs as a result of two competing mechanisms. The first one is due to shear flow which caused by the movement of one of the walls of the cavity while the second one is due to buoyancy flow produced by non-homogeneity of the cavity thermal boundaries. Understanding these mechanisms is of a great significance from technical and engineering standpoints. There were many geometric shapes of the lid-driven enclosures had been studied in the past decades considering various combinations of the imposed temperature gradients and cavity configurations. The common geometric shapes are circle, square, rectangular and triangular. However, little studies on a two-dimensional trapezoidal lid-driven enclosure have been carried out to investigate the heat transfer enhancement. These types of lid-driven enclosures are used in many engineering applications such as food processing, lubrication technologies, thermal-hydraulics of nuclear reactors, electronic cooling, crystal growth, flow and heat transfer in solar ponds, dynamics of lakes, and float glass production [1].

The mixed convection heat transfer in trapezoidal lid-driven enclosures occurred in many industrial devices using conventional fluids such as water, propylene glycol or ethylene glycol. However, the low thermal conductivity has always been the primary limitation in the development of energy-efficient heat transfer fluids, performance and compactness of many engineering equipment such as electronic devices and heat exchanger. In order to overcome this limitation, there is a strong motivation to improve advanced heat transfer fluids with substantially higher thermal conductivity. Hence, in recent years, nanofluids have attracted more attention for cooling in various industrial applications. This new generation of heat transfer fluids consists of suspended nanoparticles, which have a better suspension stability compared to millimeter or micrometer size ones. Various types of powders such as polymeric particles, non-metallic, and metallic can be added into base fluids to form slurries. Thus, the heat transfer characteristics will be enhanced by using class of fluids called nanofluids. The convective heat transfer characteristics of nanofluids depends on the thermophysical properties of the base fluid and the ultrafine particles, the flow structure, the volume fraction of suspended particles, the dimensions and the shape of these particles. Because the prospect of nanofluid is very promising, many studies on convective heat transfer using nanofluid have been reported in the recent years [2-5].

Understanding the phenomena of the recirculating flow within the cavity is treated as one of the fundamental studies to fluid-dynamics researchers and hence has been pursued extensively. Abu-Nada and Chamkha [1] studied numerically steady laminar mixed convection flow in a lid-driven inclined square enclosure filled with Al_2O_3 -water nanofluid. It was concluded that the heat transfer mechanisms and the flow characteristics inside the cavity were strongly dependent on the Richardson number. The mixed convection heat transfer

in a two-dimensional enclosure trapezoidal cavity filled with air was studied numerically by Mamun, et al. [6]. It was observed that the average Nusselt number increases with increasing the aspect ratio for all rotational angles. The average Nusselt number was also sensitive to rotational angle. Yang [7] studied numerically laminar mixed convection of air in a shear-and buoyancy-driven cavity having a locally heated lower wall and moving cooled sidewalls. It was observed that the flow and temperature fields were symmetrical about the midlength of the enclosure because of the symmetry of the boundary conditions in the vertical direction.

The mixed convection heat transfer characteristics in a lid-driven 2-D square cavity with various Richardson and Prandtl numbers was studied by Cheng [8]. It was concluded that the heat transfer increases continuously with increasing both Re and Gr numbers for $Ri = 0.01$ but it was not for $0.5 \leq Ri \leq 100$. Basak, et al. [9] studied numerically mixed convection flows in a lid-driven square cavity filled with porous medium by using penalty finite element analysis. It was concluded that the average Nusselt numbers were almost invariant with Gr number for $Pr = 0.7$ with all Da number for linearly heated side walls or cooled right wall. Basak, et al. [10] performed a numerical analysis to study the influence of linearly heated side walls or cooled right wall on mixed convection lid-driven flows in a square cavity. It was shown that (Nu_b) was equal to zero on the left edge of the bottom wall but it increases towards the right edge of the bottom wall in the cooled right wall case.

Basak, et al. [11] investigated the influence of uniform and non-uniform heating of bottom wall on mixed convection lid-driven flows in a square cavity using finite element method. It was concluded that the heat transfer rate for uniform heating was always more as compared to the non-uniform heating. Pingan, et al. [12] employed numerical method to investigate 2D laminar natural convection in a square cavity containing a circular pipe. It was concluded that the original distribution of temperature in square cavity was influenced by the quantity of heat transfer through the pipe surface. Kandaswamy, et al. [13] studied numerically the buoyancy driven convection in a square cavity induced by two mutually orthogonal and arbitrarily located baffles. It was concluded that the net heat transfer in the cavity can be enhanced by increasing the vertical baffle length regardless of its position.

Cianfrini, et al. [14] studied numerically natural convection in air-filled, tilted square enclosures. It was concluded that for a sufficiently wide range of γ around 135° the overall amount of heat transferred along the x-direction across the cavity is larger than that corresponding to the untilted case. Al-Amiri, et al. [15] studied numerically steady mixed convection in a square lid-driven cavity under the combined buoyancy effects of thermal and mass diffusion. It was found that Lewis number has insignificant effect on the isotherms and streamlines for small Richardson numbers. Ho, et al. [16] studied numerically the effects due to uncertainties in effective dynamic viscosity and thermal conductivity of the Al_2O_3 -water nanofluid on

laminar natural convection heat transfer in a square enclosure. It was observed that the uncertainties associated with different formulas adopted for the effective thermal conductivity and dynamic viscosity of the nanofluid have a strong bearing on the natural convection heat transfer characteristics in the enclosure.

Basak, et al. [17] studied numerically the steady laminar natural convection flow in a square cavity with uniformly and non-uniformly heated bottom wall using finite element method. The local Nusselt number at the bottom wall was least at the center for uniform heating and there were two minimum heat transfer zones at the center and the corner points for non-uniform heating. Moallemi and Jang [18] investigated numerically the flow and heat transfer in a lid driven square cavity. It was found that the influence of buoyancy force on the flow and heat transfer in the cavity is more pronounced for higher values of Pr number, if Re and Gr numbers are kept constant. Reima, et al. [19] studied numerically the flow of a viscous thermally-stratified fluid in a square container. It was observed that when the frequency parameter (ω') is small, the bulk of the cavity interior is affected by the oscillation of the top lid. On the contrary, when ω' was large; the flows were confined to a thin layer adjacent to the top lid.

Agrawal, et al. [20] studied numerically lid driven cavity for two different thermal boundary conditions to establish the suitability of pseudo-compressibility algorithm for mixed convection flow problems. It was concluded that the pseudo-compressibility approach was successfully applied to compute mixed convection flow inside a driven cavity for two different thermal boundary conditions. Ghasemi and Aminossadati [21] investigated numerically unsteady laminar mixed convection heat transfer in a 2D square cavity. It was concluded that the average Nusselt number for the cavity with a downwards moving wall was higher than that for the cavity with an upwards moving wall. Chamkha [22] investigated unsteady laminar combined convection flow in a square cavity in the presence of internal heat generation or absorption and a magnetic field. The flow behavior and the heat transfer characteristics inside the cavity were strongly affected by the presence of the magnetic field.

Oztop and Dagtekin [23] investigated numerically steady state laminar two-dimensional mixed convection problem in a vertical two-sided lid-driven differentially heated square cavity. When the vertical walls move upwards in the same direction (case III), the heat transfer becomes reduced compared to the other two cases. In case III, the lid opposing buoyancy forces decrease the heat transfer significantly by reducing the strength of the circulation regardless of which direction they move, both upwards or both downwards. Noor, et al. [24] studied numerically flow and heat transfer inside a square cavity with double-sided oscillating lids. Higher heat transfer rates were found at higher Reynolds number flows due to the increase of fluid activities in the bulk of the interior fluids. Vishnuvardhanarao and Das [25] investigated numerically two-dimensional steady mixed convection flow in an enclosure filled with a Darcian fluid-saturated uniform porous medium. Significant suppression of the convective currents was obtained by the presence of a porous medium.

Senthil Kumar, et al. [26] studied numerically convection driven by combined thermal and solutal concentration buoyancy effects in a lid-driven square cavity. It was observed that the position of the square blockage does affect the location of the peak value of the local Nusselt and Sherwood numbers but their average values almost remain constant. Aydm [27] investigated numerically the transport mechanism of laminar combined convection air flow in a shear-and buoyancy-driven square cavity. It was concluded that the mixed convection range of Ri number for the opposing-buoyancy case was wider than that of the aiding-buoyancy case. Sivakumar, et al. [28] studied numerically the unsteady mixed convection heat transfer and fluid flow in lid-driven cavities with different lengths of the heating portion and different locations of it. It was found that a better heat transfer rate was obtained on reducing the heating portion length in the hot wall of a differentially heated cavity.

The periodic behavior of mixed convective flow in a rectangular cavity with a vibrating lid was numerically studied by Chen and Cheng [29]. It was observed that the lid vibration effects become stronger and the effects of the natural periodic flow become weaker. Sharif [30] studied numerically laminar mixed convective heat transfer in 2D shallow rectangular driven cavities. The local Nusselt number at the cold wall exhibits oscillatory behavior near the right side due to the presence of separation bubble at the cold surface in that location. Ganzarolli and Milanez [31] studied numerically natural convection in a rectangular enclosure heated from below and symmetrically cooled from the sides, using a stream function-vorticity formulation. It was concluded that there was a little influence of the Prandtl number on the heat transfer and on the flow circulation inside the cavity.

Guo and Sharif [32] studied numerically mixed convection heat transfer in a 2D lid driven rectangular cavity filled with air subjected to a constant heat flux. It was concluded that as Ri number increases the temperature variation was restricted over a gradually diminishing region around the heat source. Luo and Yang [33] used a continuation method to calculate the flow bifurcation with/without heat transfer in a two-sided lid-driven cavity. It was demonstrated that the saddle-node bifurcation points forms a thumb-shaped boundary line which separates the stable flow states from the unstable states. Abouhamza and Pierre [34] studied numerically the hydrodynamic stability for the lid-driven cavity. It was concluded that the aspect ratio between 1 and 2, shows abrupt changes in the critical Reynolds number and the critical eigenvalues. The mixed convection in a lid driven triangular enclosure filled with a water- Al_2O_3 nanofluid was investigated numerically by Ghasemi and Aminossadati [35]. It was reported that the direction of the sliding wall motion affected the flow and temperature distribution within the enclosure and the heat transfer rate. Chen and Cheng [36] analyzed periodic flow pattern with mixed convection in a triangular cavity caused by the effects of lid oscillation and buoyancy. It was observed that the flow in the cavity may experience an oscillation at natural periodic frequencies. Three-dimensional numerical simulations of fluid flow and heat transfer in a

lid-driven cavity filled with a stably stratified fluid was investigated by Mohamad and Viskanta [37]. It was concluded that the maximum local heat transfer rate occurs at the start of the sliding lid. Three-dimensional flow structures and the heat transfer rates in double lid-driven cubic cavity was studied by Ouertatani, et al. [38]. The average heat transfer for the case of the cubic cavity with two moving lids was superior to that in the case of the cubic cavity with only one moving lid.

It is obvious from the above literature review that the case of mixed convective heat transfer in trapezoidal enclosure utilizing nanofluids seems not to have been investigated in the past and this has motivated the present study. Thus, most of the previous research on trapezoidal enclosure involved conventional fluids (not nanofluids) and there is a very little work reported in the open literature that involved nanofluids in trapezoidal enclosure. The present study deals with 2D laminar mixed convective flow in trapezoidal enclosure by using different types of nanofluids, different volume fractions, different nanoparticle diameters, different Richardson numbers, different enclosure rotational angles, different inclination sidewalls angles, various aspect ratios and different lid-driven flow direction. Results of interests such as Nusselt number, streamlines and isotherms for laminar mixed convection in trapezoidal enclosure are reported to illustrate the effect of nanofluids on these parameters.

2. Numerical Model

2.1 Physical Model

Schematic diagrams of trapezoidal lid-driven enclosure for two cases are shown in Fig. 1. The first case when the cold wall is moving in the positive x-direction (opposing flow condition). The second case when the cold wall is moving in the negative x-direction (aiding flow condition). Both the height and length of the trapezoidal lid-driven enclosure are changed with the change of the aspect ratio ($A=H/W$), inclination angle, γ or with the rotation angle, Φ .

2.2 Governing equations

It is important to set up the governing equations (continuity, momentum, and energy) to complete the CFD analysis of the trapezoidal lid-driven cavity. Using the Boussinesq approximation and neglecting the viscous dissipation effect and compressibility effect the dimensionless governing equations for two dimensional laminar incompressible flows can be written as follows [2]:

The continuity equation:

$$\frac{\partial U}{\partial X} + \frac{\partial V}{\partial Y} = 0 \quad (1)$$

X-momentum equation:

$$U \frac{\partial U}{\partial X} + V \frac{\partial U}{\partial Y} = -\frac{\partial P}{\partial X} + \frac{1}{\text{Re}} \left(\frac{\partial^2 U}{\partial X^2} + \frac{\partial^2 U}{\partial Y^2} \right) \quad (2)$$

Y-momentum equation:

$$U \frac{\partial V}{\partial X} + V \frac{\partial V}{\partial Y} = -\frac{\partial P}{\partial Y} + \frac{1}{\text{Re}} \left(\frac{\partial^2 V}{\partial X^2} + \frac{\partial^2 V}{\partial Y^2} \right) + \frac{\text{Gr}}{\text{Re}^2} \theta \quad (3)$$

Energy equation:

$$U \frac{\partial \theta}{\partial X} + V \frac{\partial \theta}{\partial Y} = \frac{1}{\text{Re.Pr}} \left(\frac{\partial^2 \theta}{\partial X^2} + \frac{\partial^2 \theta}{\partial Y^2} \right) \quad (4)$$

The dimensionless variables are as follows:

$$X = \frac{x}{W}, Y = \frac{y}{W}, \theta = (T_H - T_C) / \Delta T, \Delta T = \frac{q'' W}{K}, U = \frac{u}{U_0}, V = \frac{v}{U_0}, \text{ and } P = \frac{p}{\rho U_0^2}.$$

2.3 Boundary conditions

The boundary conditions for the present problem are specified for the computational domain as shown in Fig. 1. These figures show the general trapezoidal lid-driven cavity model, whose bottom wall and top wall are subjected to heat flux (q'') and cold temperature (T_C) respectively while the side walls are kept adiabatic. Two cases of thermal boundary conditions for the top moving wall were considered. The first case is accounted when the cold wall is moving in the positive x-direction (opposing flow condition). In that case the shear flow caused by moving top wall opposes the buoyancy driven flow caused by the thermal non-homogeneity of the cavity boundaries. The second case is accounted when the cold wall is moving in the negative x-direction (aiding flow condition). In that case the shear flow assists the buoyancy flow. The cavity height is 'H', width of the bottom hot wall is 'W', and it is inclined with an angle Φ with the horizontal reference axis. The inclination angle of the sidewalls of the cavity is γ . The flow and heat transfer phenomena in the cavity are investigated for a series of Richardson numbers (Ri), aspect ratio ($A=H/W$), and rotation angle of the cavity Φ .

2.4 Grid independence test and code validation

In this section, grid independence test is carried out to obtain the most suitable mesh faces size for this particular geometry. In this study, four mesh faces are considered 5470, 7170, 8942 and 11064 at $Ri=1$, $Re=400$ and $A=1$. The discretization grid is unstructured and non-uniform. It is observed that all the four mesh faces has similar results of Nusselt number. However, any one of the four mesh faces can be used. In

this case, mesh faces (5470) is used as it is the best in the terms of both the accuracy and computational time.

2.5 Code validation

The present results were validated with the results of Mamun, et al. [6] who have studied mixed convection air flow in trapezoidal lid-driven cavity heated from the bottom wall. In addition, another study of Guo and Sharif [32] was selected to be surer of code validation. They studied mixed convection heat transfer in rectangular cavity with constant heat flux heated from the bottom wall, while the isothermal sidewalls are moving downward with uniform velocity and are kept at a constant temperature. Moreover, their research was about using two-phase mixture model on the nanofluid within two sided lid driven enclosure. The comparison of the present results of Nusselt number variation with different (A) with the results of Guo and Sharif [32], and Mamun, et al. [6] is shown in Fig. 2a. It is clearly seen that the present results are in excellent agreement with the range of aspect ratio 0.5 - 2. Furthermore, attainment of the code validation comparisons in terms of isotherms and streamlines were also carried out. The isotherms and streamlines were obtained for different Richardson numbers in the range of 0.1 - 10 as shown in Fig. 2b-c. In addition, validation of nanofluids have been completed in this paper as well. As plotted in Fig. 2d, the current results are also provided a great endorsement with those obtained by Alinia, et al. [39]. The comparison shows excellent agreement between the present results and the results of Mamun, et al. [6] and Guo and Sharif [32] as shown in Fig. 2a-c.

2.6 Numerical procedure

The numerical computations were carried out by solving the governing conservations along with the boundary conditions by using Finite Volume Method (FVM) [40]. The second-order upwind differencing scheme is considered for the convective terms. The diffusion term in the momentum and energy equations is approximated by second-order central difference which gives a stable solution. The dimensionless physical parameters were calculated from the computed velocity and temperature distributions. The flow field was solved using the SIMPLE algorithm [40]. This is an iterative solution procedure where the computation is initialized by guessing the pressure field. Then, the momentum equation is solved to determine the velocity components. The pressure is updated using the continuity equation. Even though the continuity equation does not contain any pressure, it can be transformed easily into a pressure correction equation [40]. The iterations were continued until the sum of residuals for all computational cells became negligible 10^{-5} and velocity components did not change from iteration to iteration. Because of the assumption of constant fluid properties and negligible buoyancy, the mass and momentum equations were not coupled to the energy equation. Therefore, the temperature field was calculated by solving the energy

equation after a converged solution for the flow field was obtained by solving the momentum and continuity equations.

2.7 Thermophysical properties of nanofluids

The effective thermophysical properties of nanofluids were calculated using the following equations:

The effective thermal conductivity can be obtained by using the following mean empirical correlation [41]:

$$k_{\text{eff}} = k_{\text{Static}} + k_{\text{Brownian}} \quad (5)$$

$$k_{\text{Static}} = k_f \left[\frac{(k_{\text{np}} + 2k_f) - 2\phi(k_f - k_{\text{np}})}{(k_{\text{np}} + 2k_f) + \phi(k_f - k_{\text{np}})} \right] \quad (5.1)$$

$$k_{\text{Brownian}} = 5 \times 10^4 \beta \phi \rho_f C_{p,f} \sqrt{\frac{k T}{2\rho_{\text{np}} R_{\text{np}}}} f(T, \phi) \quad (5.2)$$

where: Boltzmann constant: $k = 103807 \times 10^{-23}$ J/K

Modelling function, β : $\beta = 0.0137(100\phi)^{-0.8229}$ for $\phi < 1\%$, $\beta = 0.0011(100\phi)^{-0.7272}$ for $\phi > 1\%$

Modeling, $f(T, \phi)$:

$f(T, \phi) = (-6.04\phi + 0.4075)T + (1722.3\phi)$ for $1\% \leq \phi \leq 4\%$ and $300 \text{ K} < T < 325 \text{ K}$

The effective viscosity can be obtained by using the following mean empirical correlation [41]:

$$\mu_{\text{eff}} = \mu_{\text{Static}} + \mu_{\text{Brownian}} \quad (6)$$

$$\mu_{\text{Static}} = \mu_f / (1 - \phi)^{2.5} \quad (6.1)$$

$$\mu_{\text{Brownian}} = 5 \times 10^4 \beta \phi \rho_f \sqrt{\frac{k T}{2\rho_{\text{np}} R_{\text{np}}}} f(T, \phi) \quad (6.2)$$

where Boltzmann constant: $\beta = 0.0137(100\phi)^{-0.8229}$ for $\phi < 1\%$

$\beta = 0.0011(100\phi)^{-0.7272}$ for $\phi > 1\%$

Modeling, $f(T, \phi)$: $f(T, \phi) = (-6.04\phi + 0.4075)T + (1722.3\phi)$ for $1\% \leq \phi \leq 4\%$
and $300 \text{ K} < T < 325 \text{ K}$

The density of the nanofluid, ρ_{nf} can be obtained from the following equation [41]:

$$\rho_{nf} = (1 - \phi)\rho_f + \phi\rho_{\text{np}} \quad (7)$$

where ρ_f and ρ_{np} are the mass densities of the base fluid and the solid nanoparticles, respectively.

The effective heat capacity at constant pressure of the nanofluid $(\rho C_p)_{nf}$ can be calculated from the following equation [41]:

$$(\rho C_p)_{nf} = (1 - \phi)(\rho C_p)_f + \phi(\rho C_p)_{\text{np}} \quad (8)$$

where, $(\rho C_p)_f$ and $(\rho C_p)_{np}$ are the heat capacities of base fluid and nanoparticles, respectively.

The effective coefficient of thermal expansion of nanofluid $(\rho\beta)_{nf}$ can be obtained from the following equation [37]:

$$(\rho\beta)_{nf} = (1 - \phi)(\rho\beta)_f + \phi(\rho\beta)_{np} \quad (9)$$

where $(\rho\beta)_f$ and $(\rho\beta)_{np}$ are thermal expansion coefficients of base fluid and nanoparticles, respectively.

The thermophysical properties of different types of nanoparticle are listed in [Table 1](#).

3. Results and discussion

This section presents all the relevant numerical results for mixed convection heat transfer in a trapezoidal lid-driven cavity under different parameters such as the types of nanofluids, volume fractions of nanoparticles, diameters of nanoparticles, Richardson number, rotational angle, inclination angle, aspect ratio and direction of moving cold wall. The results are presented in terms of Nusselt number on the bottom wall, isotherms and streamlines.

3.1 The effect of nanoparticle types

Four different types of nanoparticles Al_2O_3 , CuO , SiO_2 , and TiO_2 and pure water as a base fluid are used. The Nusselt number for different nanofluids at aspect ratio = 1, $Re = 100$ and different values of Ri (0.1, 1, 5 and 10) are shown in [Fig. 3a-d](#) respectively. It is observed that all nanofluids possess higher Nusselt number compared to pure water. These results also indicate that all the four types of nanofluids are comparatively richer in heat transfer rate than the pure water. In addition, it is clear that the SiO_2 nanofluid has the best heat transfer rate, followed by Al_2O_3 , TiO_2 and CuO respectively. This is because SiO_2 has the lowest thermal conductivity than the other nanofluids, but higher than water and has the highest average velocity among the fluids due to its lowest density compared with the others. The fluid velocity plays an important role on the heat transfer in case of mixed convection and it represents the main reason to give high heat transfer coefficient. It can also be seen that the Nu number increased by increasing Ri number as shown in [Fig. 3a-d](#).

3.2 The effect of nanoparticle volume fractions

The effect of nanoparticle volume fraction in the range of 1 - 4% with different values of Richardson numbers at $Re = 100$, with opposing flow case on the Nusselt number is shown in [Fig. 4a-c](#). The results

show that increasing nanoparticles volume fraction enhances the Nusselt number. This is because as the volume fraction increases, irregular and random movements of particles increases the energy exchange rates in the fluid with penalty on the wall shear stress and consequently enhance the thermal dispersion of the flow. In each case of volume fraction, the Nu number increases as Ri number increases.

3.3 *The effect of nanoparticle diameters*

This study is used SiO₂-water as a working fluid with fixed other parameters such as inclination angle of sidewalls 30°, Re = 100 and volume fraction 4% except Richardson number was in the range of 0.1 - 10. The range of nanoparticles diameter considered is 25 - 70 nm. As illustrated in Fig. 5a-c, the results show that the nanofluid with smaller particle diameter have the higher Nusselt number. The effect of particle size may be attributed mainly to two reasons which are the high specific surface area of the nanoparticles and the Brownian motion. As the particle size reduces, the surface area per unit volume increases, the heat transfer is being dependent on the surface area, and thus the effectiveness of nanoparticles in transferring heat to the base liquid increases. However, reducing the particle size means increasing the Brownian motion velocity, which again adds up to the contribution by the nanoparticles to the total heat transfer by continuously creating additional paths for the heat flow in the fluid. As presented in this figure the nanofluid with 25nm nanoparticle diameter has the highest Nusselt number, whereas, the nanoparticle with a diameter of 70 nm has the lowest Nusselt number. In all cases, it can be observed that Nu number increases with increasing Ri number for all nanoparticles diameters.

3.4 *The effect of rotational angles*

The effect of rotational angle, Φ was studied with different Ri numbers with fixed value of Re = 100 and under opposing flow condition with inclination sidewalls angle of 30°. As shown in (b)

Fig. 6a, the results show that the Nu_{av} is sensitive to the rotational angle. It can be seen that the Nu number increases as the rotational angle, Φ decreases from 60° - 30°. This phenomenon can be ascribed to the fact that the lid-driven becomes more active to enhance the heat transfer.

The effect of the rotational angle on the streamlines and isotherms is also presented in (b)

Fig. 6b for different Ri numbers. These figures show that as Ri number increases ($Ri > 1$) natural convection is starting to create circulation at the bottom wall of the cavity. This circulation casting by natural convection goes bigger and stronger as Ri number increases as well as squeezes the upper circulation. The isotherms maps change accordingly with streamlines, and as Ri number increases the isotherm map changes

significantly, that indicating the natural convection is the dominating heat transfer for this particular case. On the other hand, the shear driven circulation at the upper right side becomes smaller and smaller with Ri number increment because of the dominating of the natural convection. By increasing the rotation angle, the natural convection started to become dominating with smaller Ri number comparing with the smaller angle of rotation as shown in (b)

Fig. 6b.

3.5 The effect of sidewalls inclination angles

The effect of inclination angles of the adiabatic sidewalls on the Nusselt number is investigated and shown in (b)

Fig. 7a. The inclination angle is varied from 30° to 60° of the sidewalls with several values of Ri number in the range of 0.1 - 10. The results are obtained at $Re = 100$ and opposing flow case. The results show that the Nusselt number is higher at $\gamma = 30^\circ$. This phenomenon can be ascribed to the fact that the lid-driven becomes more active to enhance the heat transfer. In other words, by decreasing the inclination angle the length of lid-driven wall is increased and this would lead to enhance the heat transfer.

The impact of varying the inclination angles of the sidewalls of the trapezoidal enclosure at different Ri numbers on the streamlines and isotherms are shown in (b)

Fig. 7b at $\gamma = 30^\circ$. For the small values of Ri number, it can be seen that the shear effect due to the movement of the top wall is dominant. The fluid flow is characterized by a primary recirculating eddy of the size of the cavity generated by the movement of the top lid. The isothermal contour maps are clustered near the bottom and top walls resulting in steep temperature gradient there. By increasing the inclination angle (γ) the maps of the streamlines and isotherms become more dominate. In each case as the Ri number increases the convection current becomes more dominant resulting in stronger flow field.

3.6 The effects of aspect ratios and flow direction

The effect of different aspect ratios (A) in the range of 0.5 - 2 of the cavities on the Nusselt number is shown in Fig. 8a for an inclination angle of sidewalls of 30° and for opposing flow case. Richardson number was in the range of 0.1 to 10 with keeping Reynolds number at 100. The results show that the Nusselt number increased by increasing the aspect ratio. It is observed that in the convection region adjacent to the heat

source, the isotherms become thinner and denser producing higher temperature gradients with increasing the aspect ratio. This is due to the fact that the cavity volume increases with aspect ratio and more volume of cooling fluid is involved in cooling the heat source and this leads to better cooling effect.

The effect of thermal boundary conditions for the top moving wall is shown in Fig. 8b for opposing and aiding flow conditions at $\Phi = 30^\circ$ and $Re = 100$. The results show that the Nusselt number of aiding flow is higher than that for opposing flow. This is because for aiding flow the body force has same direction as the shear driven flow direction, which accelerates the fluid resulting in an increase of the Nusselt number. However, for opposing flow, the body force acts opposite to the shear driven flow direction, thus retarding the flow and possibly causing flow reversal in the upper part of the cross-section. Therefore, the Nusselt number results for opposing flow were lower than that the aiding flow. As Ri number increases, the convection flow fields become more stronger resulting in better heat transfer.

4. Conclusions

The problem of steady laminar mixed convective flow and heat transfer of different types of nanofluids made up of water and Al_2O_3 , CuO , SiO_2 , and TiO_2 in a lid-driven trapezoidal enclosure was formulated and solved numerically using a second-order accurate finite-volume method. The method is validated by direct comparisons with previously published work on special cases of the problem and the results are found to be in good agreement. Graphical results for various parametric conditions were presented and discussed. It was found that the heat transfer mechanisms and the flow characteristics inside the enclosure are strongly dependent on the Richardson number. The results show that SiO_2 gives the highest Nusselt number followed by Al_2O_3 , TiO_2 and CuO , respectively while pure water gives the lowest Nusselt number. The Nusselt number increased with increasing the volume fraction of nanoparticles and the aspect ratio and decreasing the nanoparticles diameter. The Nusselt number is sensitive to the rotational angle (Φ), and it increases when Φ decreases and the inclination angle (γ) decreases from $30^\circ - 60^\circ$, at all values of Richardson number. The direction of the motion of the lid-driven affects the heat transfer phenomena. Aiding flow condition always gives better heat transfer rate than opposing flow condition.

Table Captions

Table 1: The thermophysical properties of water and different nanoparticles at $T = 293$ K.

Thermophysical properties	Water	Al_2O_3	CuO	TiO_2	SiO_2
Density, ρ (kg/m ³)	998.203	3970	6500	4250	2200
Dynamic viscosity, μ (Ns/m ²)	1.01×10^{-3}	-	-	-	-
Thermal conductivity, k (W/m.K)	0.613	40	20	8.9538	1.2
Specific heat, c_p (J/kg.K)	4182.2	765	535.6	686.2	703
Coefficient of thermal expansion, β (1/K)	2.06×10^{-4}	5.8×10^{-6}	4.3×10^{-6}	1.7×10^{-6}	5.5×10^{-6}

Figures Captions

- Fig. 1. Schematic diagram of the trapezoidal cavity. 16
- Fig. 2. Comparison of the present results with the results of Mamun et al. Mamun, et al. [6], and Guo and Sharif [32] (a) Nusselt number at $Ri = 0.1$ and 10 , $Re=100$ and $\varepsilon = 0.6$, (b) Isotherms at $Re = 400$, $A = 1$ and $\gamma = 30^\circ$, (c) Streamlines at $Re = 400$, $A = 1$ and $\gamma = 30^\circ$ (d) The average Nusselt number comparison of naonfluid volume fraction of the present work with Alinia, et al. [39] work. 17
- Fig. 3. Variation of Nusselt number with x-position for different nanofluids types at $Re = 100$, (a) $Ri = 0.1$, (b) $Ri = 1$, (c) $Ri = 5$ and (d) $Ri = 10$ 18
- Fig. 4. Nusselt number with x-position for different volume fractions at $Re=100$, (a) $Ri = 0.1$, (b) $Ri = 3$, (c) $Ri = 10$ 19
- Fig. 5. Variation of Nusselt number with x-position for different nanoparticle diameters at $Re=100$, (a) $Ri = 0.1$, (b) $Ri = 3$, (c) $Ri = 10$ 20
- Fig. 6. (a) Average Nusselt number with Ri number at different rotational angles at $Re = 100$, (b) Streamlines (left) and isotherms (right) for different Richardson numbers at $\Phi = 30^\circ$ 21
- Fig. 7. (a) Average Nusselt number with Richardson number for different inclination angles at $Re=100$, (b) Streamlines (left) and isotherms (right) for different Richardson numbers at $\gamma = 30^\circ$ 22
- Fig. 8. (a) Average Nusselt number with Richardson number for different aspect ratios at $Re=100$, (b) Average Nusselt number with Richardson number for different flow directions at $Re=100$ and $\Phi = 30^\circ$. 23

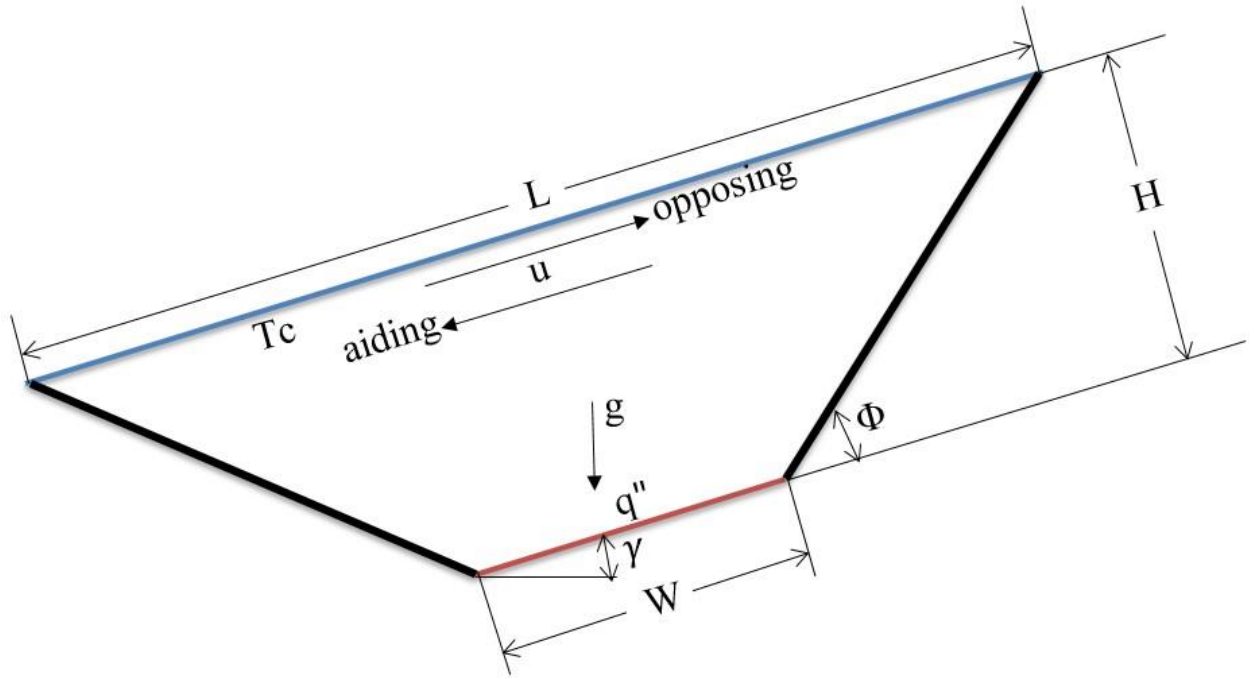
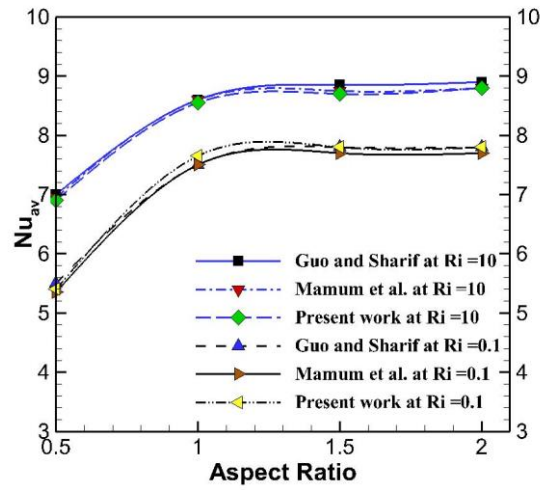
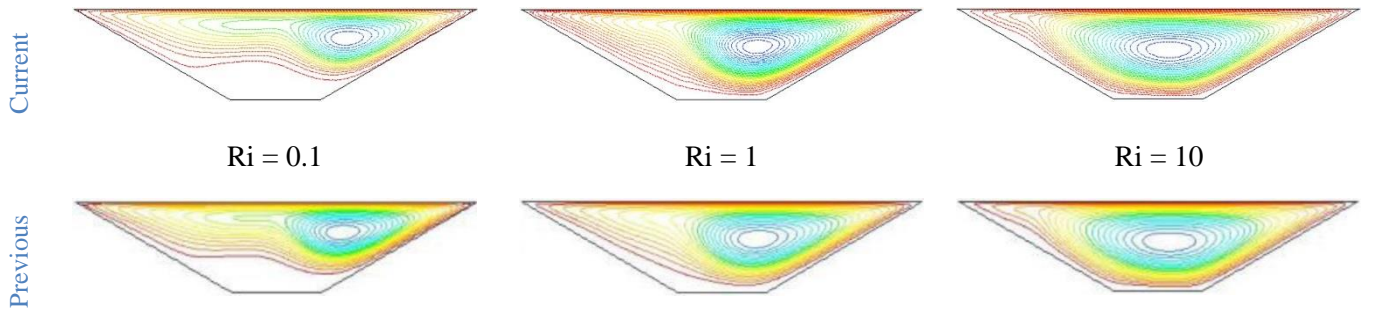


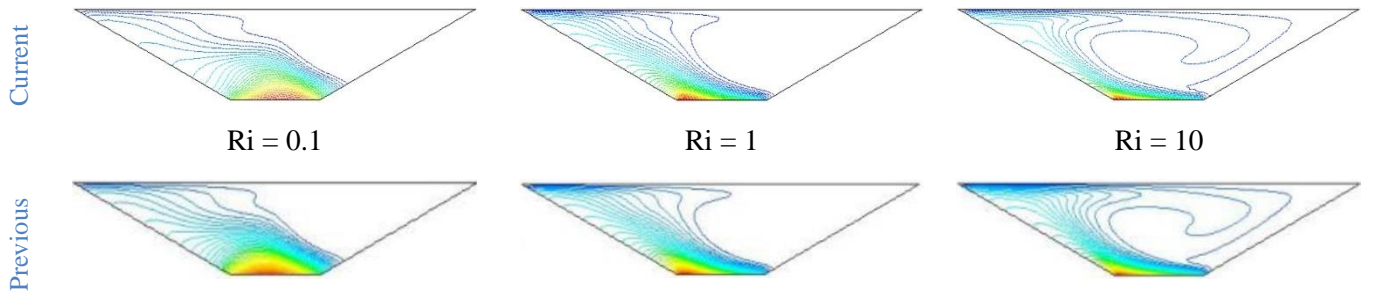
Fig. 1. Schematic diagram of the trapezoidal cavity.



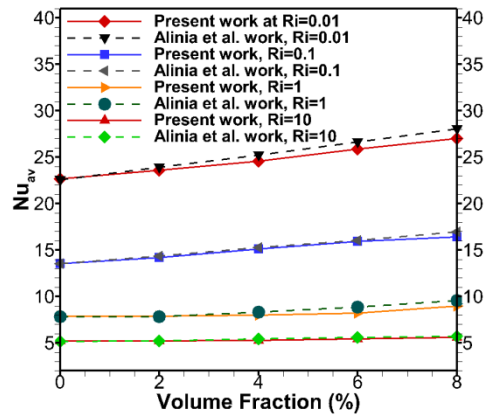
(a)



(b)

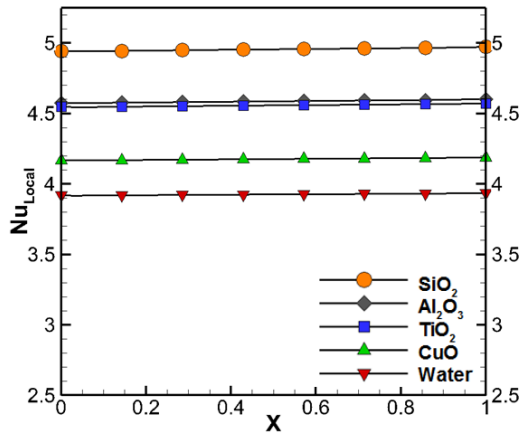


(c)

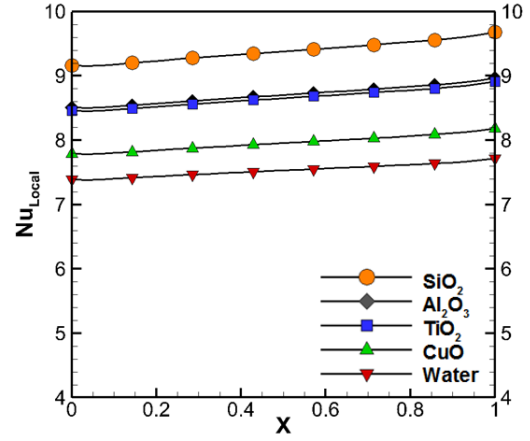


(d)

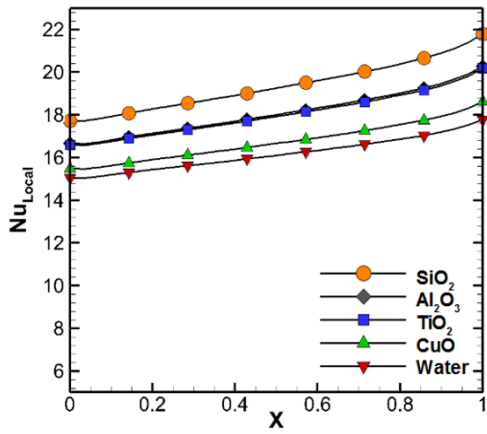
Fig. 2. Comparison of the present results with the results of Mamun et al. Mamun, et al. [6], and Guo and Sharif [32] (a) Nusselt number at $Ri = 0.1$ and 10 , $Re=100$ and $\epsilon = 0.6$, (b) Isotherms at $Re = 400$, $A = 1$ and $\gamma = 30^\circ$, (c) Streamlines at $Re = 400$, $A = 1$ and $\gamma = 30^\circ$ (d) The average Nusselt number comparison of naonfluid volume fraction of the present work with Alinia, et al. [39] work.



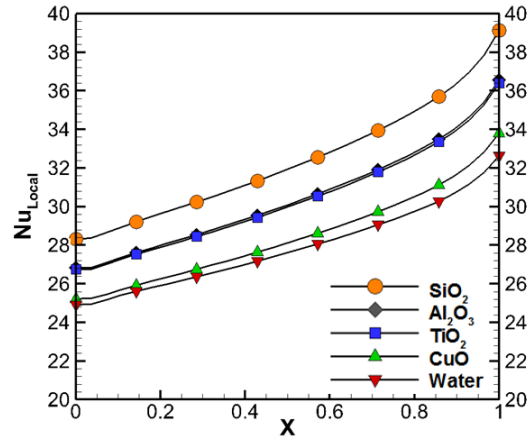
(a)



(b)

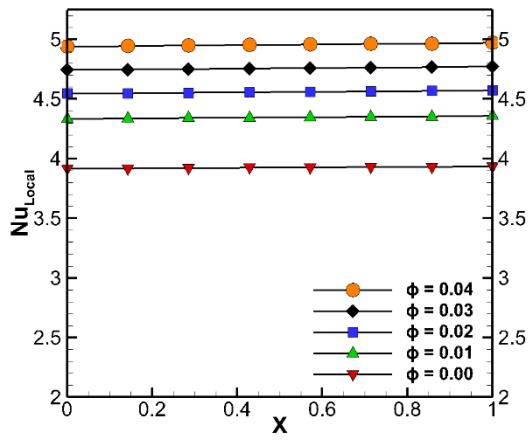


(c)

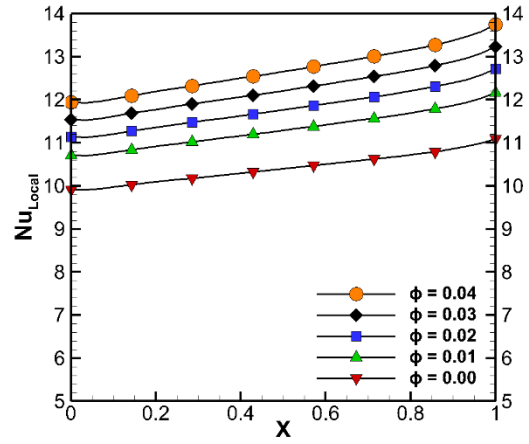


(d)

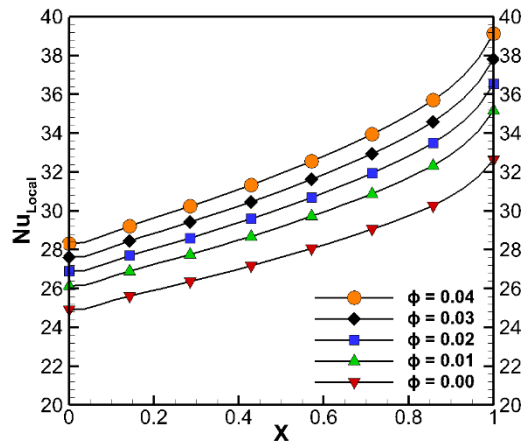
Fig. 3. Variation of Nusselt number with x-position for different nanofluids types at Re = 100, (a) Ri = 0.1, (b) Ri = 1, (c) Ri = 5 and (d) Ri = 10



(a)

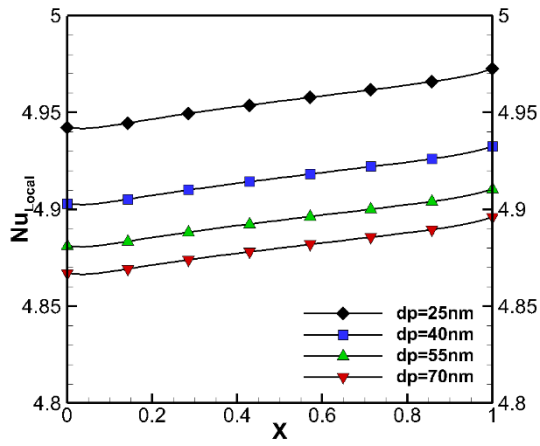


(b)

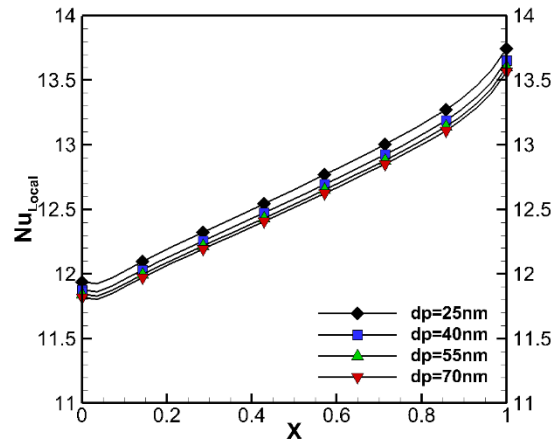


(c)

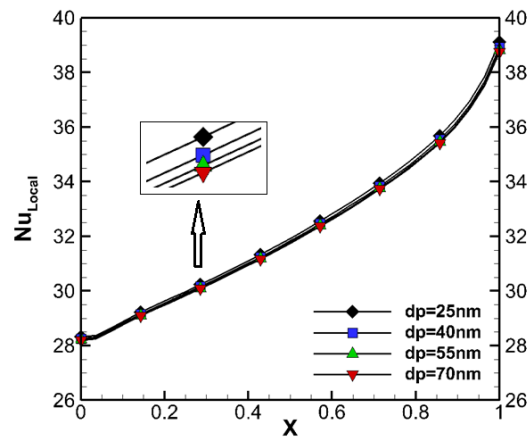
Fig. 4. Nusselt number with x-position for different volume fractions at Re=100, (a) Ri = 0.1, (b) Ri = 3, (c) Ri = 10



(a)

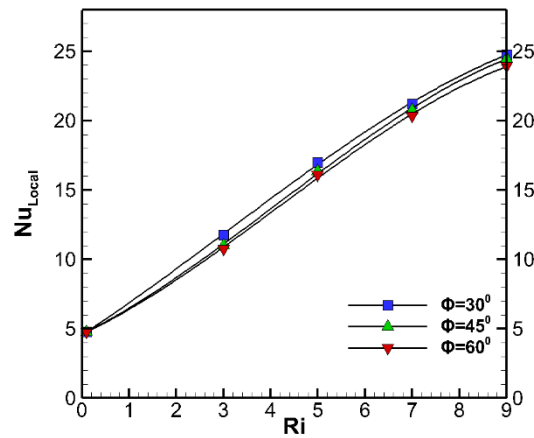


(b)



(c)

Fig. 5. Variation of Nusselt number with x -position for different nanoparticle diameters at $Re=100$, (a) $Ri=0.1$, (b) $Ri=3$, (c) $Ri=10$



(a)

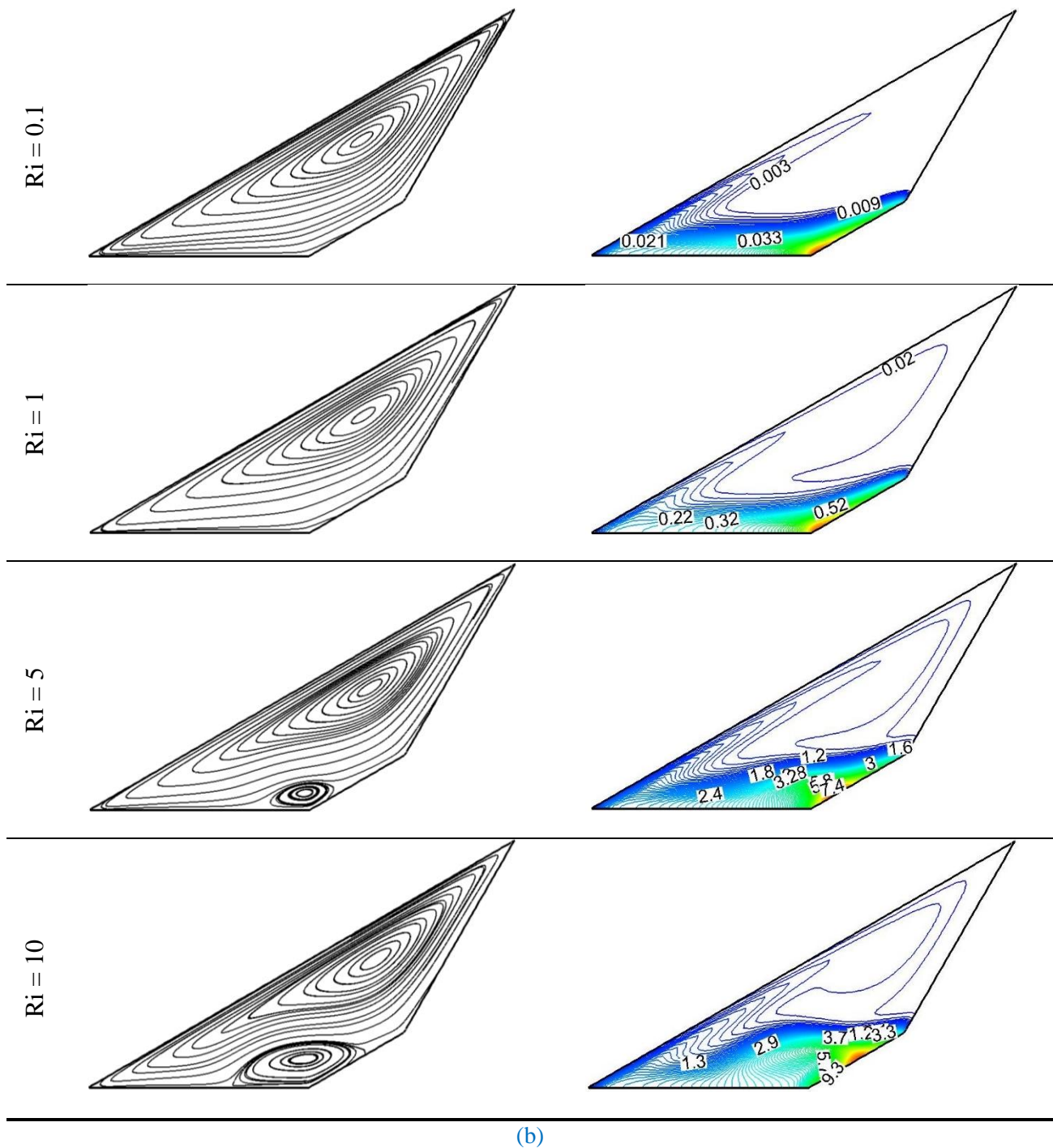
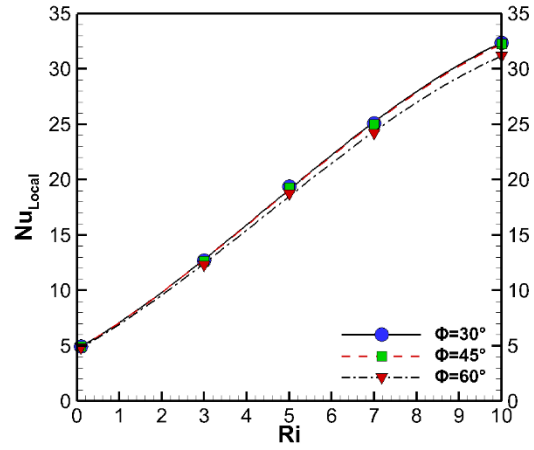
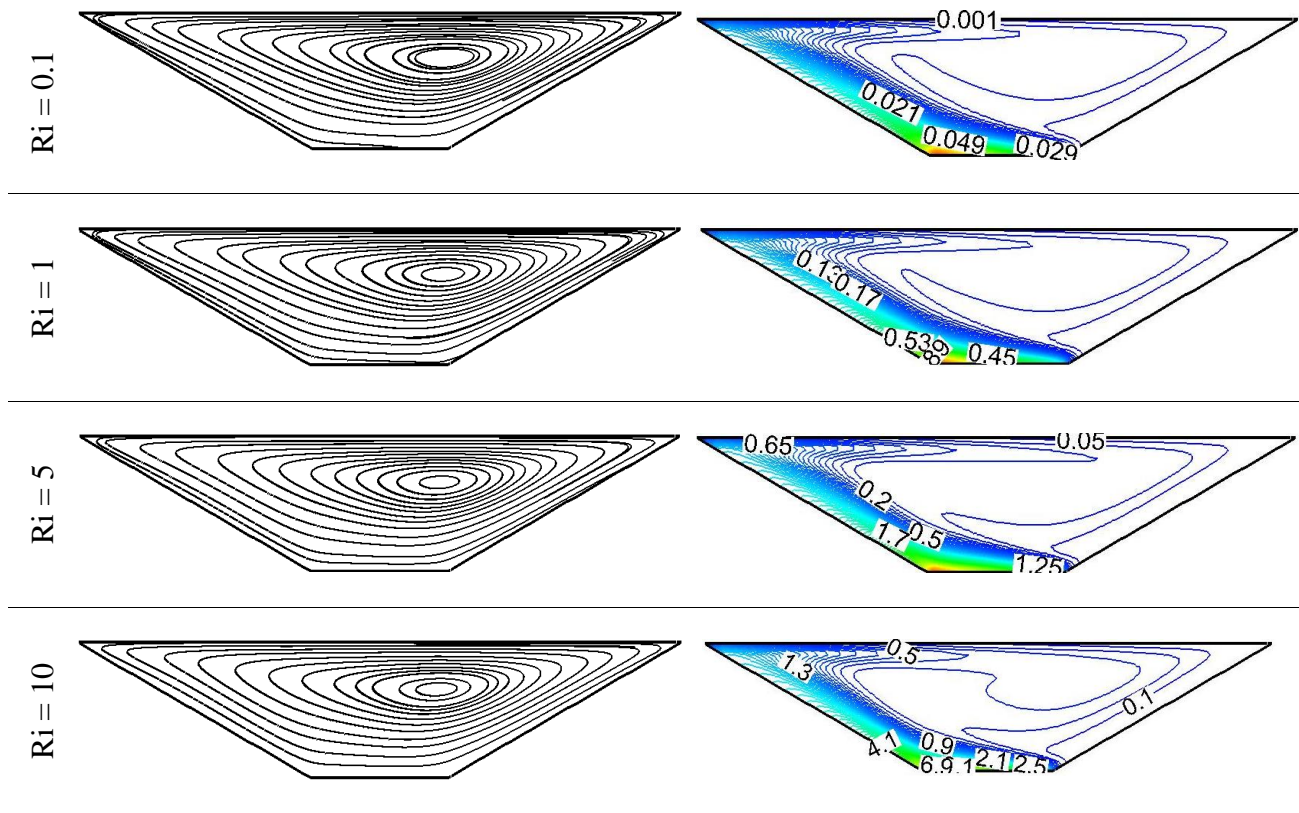


Fig. 6. (a) Average Nusselt number with Ri number at different rotational angles at $Re = 100$, (b) Streamlines (left) and isotherms (right) for different Richardson numbers at $\Phi = 30^\circ$

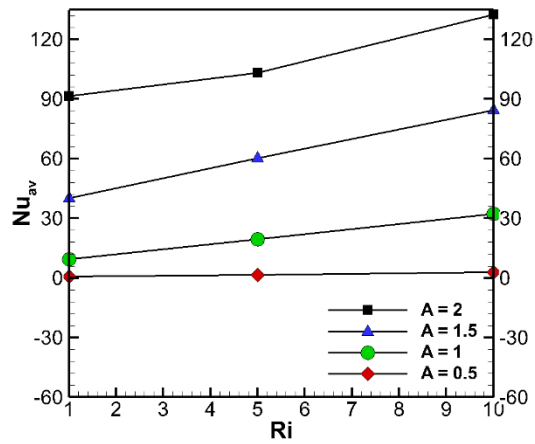


(a)

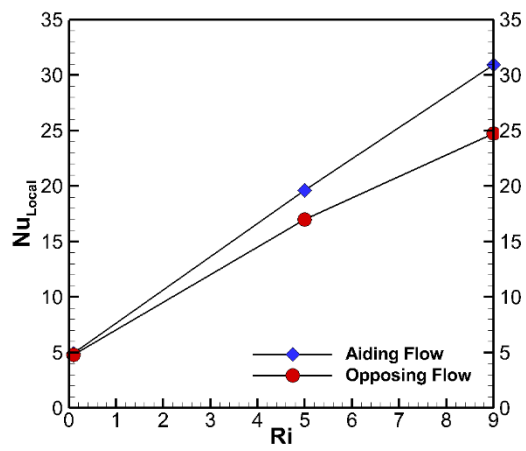


(b)

Fig. 7. (a) Average Nusselt number with Richardson number for different inclination angles at $Re=100$, (b) Streamlines (left) and isotherms (right) for different Richardson numbers at $\gamma = 30^\circ$



(a)



(b)

Fig. 8. (a) Average Nusselt number with Richardson number for different aspect ratios at $Re=100$, (b) Average Nusselt number with Richardson number for different flow directions at $Re=100$ and $\Phi = 30^\circ$

References

- [1] E. Abu-Nada, A.J. Chamkha, Mixed convection flow in a lid-driven inclined square enclosure filled with a nanofluid, *European Journal of Mechanics-B/Fluids*, 29(6) (2010) 472-482.
- [2] H. Mohammed, A. Al-Aswadi, N. Shuaib, R. Saidur, Convective heat transfer and fluid flow study over a step using nanofluids: a review, *Renewable and Sustainable Energy Reviews*, 15(6) (2011) 2921-2939.
- [3] H. Mohammed, G. Bhaskaran, N. Shuaib, R. Saidur, Heat transfer and fluid flow characteristics in microchannels heat exchanger using nanofluids: a review, *Renewable and Sustainable Energy Reviews*, 15(3) (2011) 1502-1512.
- [4] R. Saidur, S. Kazi, M. Hossain, M. Rahman, H. Mohammed, A review on the performance of nanoparticles suspended with refrigerants and lubricating oils in refrigeration systems, *Renewable and Sustainable Energy Reviews*, 15(1) (2011) 310-323.
- [5] R. Saidur, K. Leong, H. Mohammad, A review on applications and challenges of nanofluids, *Renewable and sustainable energy reviews*, 15(3) (2011) 1646-1668.
- [6] M. Mamun, T. Tanim, M. Rahman, R. Saidur, S. Nagata, Mixed convection analysis in trapezoidal cavity with a moving lid, *International Journal of Mechanical and Materials Engineering*, 5(1) (2010) 18-28.
- [7] O.A. Yang, Wen-Jei, Mixed convection in cavities with a locally heated lower wall and moving sidewalls, *Numerical Heat Transfer: Part A: Applications*, 37(7) (2000) 695-710.
- [8] T. Cheng, Characteristics of mixed convection heat transfer in a lid-driven square cavity with various Richardson and Prandtl numbers, *International Journal of Thermal Sciences*, 50(2) (2011) 197-205.
- [9] T. Basak, S. Roy, S.K. Singh, I. Pop, Analysis of mixed convection in a lid-driven porous square cavity with linearly heated side wall (s), *International Journal of Heat and Mass Transfer*, 53(9) (2010) 1819-1840.
- [10] T. Basak, S. Roy, P.K. Sharma, I. Pop, Analysis of mixed convection flows within a square cavity with linearly heated side wall (s), *International Journal of Heat and Mass Transfer*, 52(9) (2009) 2224-2242.
- [11] T. Basak, S. Roy, P.K. Sharma, I. Pop, Analysis of mixed convection flows within a square cavity with uniform and non-uniform heating of bottom wall, *International Journal of Thermal Sciences*, 48(5) (2009) 891-912.
- [12] L. Pingan, G. Ye, M. Hairong, H. Liu, Numerical simulations on natural convection in a square cavity containing a circular pipe, in: *Computer Design and Applications (ICCD), 2010 International Conference on*, IEEE, 2010, pp. V3-485-V483-489.
- [13] P. Kandaswamy, J. Lee, A.A. Hakeem, S. Saravanan, Effect of baffle–cavity ratios on buoyancy convection in a cavity with mutually orthogonal heated baffles, *International Journal of Heat and Mass Transfer*, 51(7) (2008) 1830-1837.
- [14] C. Cianfrini, M. Corcione, P.P. Dell'Omo, Natural convection in tilted square cavities with differentially heated opposite walls, *International journal of thermal sciences*, 44(5) (2005) 441-451.
- [15] A.M. Al-Amiri, K.M. Khanafer, I. Pop, Numerical simulation of combined thermal and mass transport in a square lid-driven cavity, *International journal of thermal sciences*, 46(7) (2007) 662-671.
- [16] C.-J. Ho, M. Chen, Z. Li, Numerical simulation of natural convection of nanofluid in a square enclosure: effects due to uncertainties of viscosity and thermal conductivity, *International Journal of Heat and Mass Transfer*, 51(17) (2008) 4506-4516.
- [17] T. Basak, S. Roy, A. Balakrishnan, Effects of thermal boundary conditions on natural convection flows within a square cavity, *International Journal of Heat and Mass Transfer*, 49(23) (2006) 4525-4535.
- [18] M. Moallemi, K. Jang, Prandtl number effects on laminar mixed convection heat transfer in a lid-driven cavity, *International Journal of Heat and Mass Transfer*, 35(8) (1992) 1881-1892.
- [19] I. Reima, J.M. Hyun, K. Kuno, Convection in a differentially-heated square cavity with a torsionally-oscillating lid, *International journal of heat and mass transfer*, 35(5) (1992) 1069-1076.
- [20] L. Agrawal, J. Mandal, A. Marathe, Computations of laminar and turbulent mixed convection in a driven cavity using pseudo-compressibility approach, *Computers & fluids*, 30(5) (2001) 607-620.

- [21] B. Ghasemi, S. Aminossadati, Comparison of mixed convection in a square cavity with an oscillating versus a constant velocity wall, *Numerical Heat Transfer, Part A: Applications*, 54(7) (2008) 726-743.
- [22] A.J. Chamkha, Hydromagnetic combined convection flow in a vertical lid-driven cavity with internal heat generation or absorption, *Numerical Heat Transfer: Part A: Applications*, 41(5) (2002) 529-546.
- [23] H.F. Oztop, I. Dagtekin, Mixed convection in two-sided lid-driven differentially heated square cavity, *International journal of heat and mass transfer*, 47(8) (2004) 1761-1769.
- [24] D.Z. Noor, P.R. Kanna, M.-J. Chern, Flow and heat transfer in a driven square cavity with double-sided oscillating lids in anti-phase, *International Journal of Heat and Mass Transfer*, 52(13) (2009) 3009-3023.
- [25] E. Vishnuvardhanarao, M.K. Das, Laminar mixed convection in a parallel two-sided lid-driven differentially heated square cavity filled with a fluid-saturated porous medium, *Numerical Heat Transfer, Part A: Applications*, 53(1) (2007) 88-110.
- [26] D. Senthil Kumar, K. Murugesan, H. Thomas, Numerical simulation of double diffusive mixed convection in a lid-driven square cavity using velocity-vorticity formulation, *Numerical Heat Transfer, Part A: Applications*, 54(9) (2008) 837-865.
- [27] O. Aydm, Aiding and opposing mechanisms of mixed convection in a shear-and buoyancy-driven cavity, *International communications in heat and mass transfer*, 26(7) (1999) 1019-1028.
- [28] V. Sivakumar, S. Sivasankaran, P. Prakash, J. Lee, Effect of heating location and size on mixed convection in lid-driven cavities, *Computers & Mathematics with Applications*, 59(9) (2010) 3053-3065.
- [29] C.-L. Chen, C.-H. Cheng, Numerical simulation of periodic mixed convective heat transfer in a rectangular cavity with a vibrating lid, *Applied Thermal Engineering*, 29(14) (2009) 2855-2862.
- [30] M. Sharif, Laminar mixed convection in shallow inclined driven cavities with hot moving lid on top and cooled from bottom, *Applied thermal engineering*, 27(5) (2007) 1036-1042.
- [31] M.M. Ganzarolli, L.F. Milanez, Natural convection in rectangular enclosures heated from below and symmetrically cooled from the sides, *International Journal of Heat and Mass Transfer*, 38(6) (1995) 1063-1073.
- [32] G. Guo, M.A. Sharif, Mixed convection in rectangular cavities at various aspect ratios with moving isothermal sidewalls and constant flux heat source on the bottom wall, *International journal of thermal sciences*, 43(5) (2004) 465-475.
- [33] W.-J. Luo, R.-J. Yang, Multiple fluid flow and heat transfer solutions in a two-sided lid-driven cavity, *International journal of heat and mass transfer*, 50(11) (2007) 2394-2405.
- [34] A. Abouhamza, R. Pierre, A neutral stability curve for incompressible flows in a rectangular driven cavity, *Mathematical and computer modelling*, 38(1) (2003) 141-157.
- [35] B. Ghasemi, S. Aminossadati, Mixed convection in a lid-driven triangular enclosure filled with nanofluids, *International Communications in Heat and Mass Transfer*, 37(8) (2010) 1142-1148.
- [36] C.-L. Chen, C.-H. Cheng, Numerical study of the effects of lid oscillation on the periodic flow pattern and convection heat transfer in a triangular cavity, *International Communications in Heat and Mass Transfer*, 36(6) (2009) 590-596.
- [37] A. Mohamad, R. Viskanta, Flow and heat transfer in a lid-driven cavity filled with a stably stratified fluid, *Applied mathematical modelling*, 19(8) (1995) 465-472.
- [38] N. Ouertatani, N.B. Cheikh, B.B. Beya, T. Lili, A. Campo, Mixed convection in a double lid-driven cubic cavity, *International Journal of Thermal Sciences*, 48(7) (2009) 1265-1272.
- [39] M. Alinia, D. Ganji, M. Gorji-Bandpy, Numerical study of mixed convection in an inclined two sided lid driven cavity filled with nanofluid using two-phase mixture model, *International Communications in Heat and Mass Transfer*, 38(10) (2011) 1428-1435.
- [40] S. Patankar, *Numerical heat transfer and fluid flow*, CRC press, 1980.
- [41] B. Ghasemi, S. Aminossadati, Brownian motion of nanoparticles in a triangular enclosure with natural convection, *International Journal of Thermal Sciences*, 49(6) (2010) 931-940.